New fluorescent derivatives from papaverine: Two mechanisms to increase the quantum yield

New Fluorescent Derivatives from Papaverine: Two Mechanisms to Increase the Quantum Yield

M. Giordano,[a] G. Volpi,[a*] C. Garino,[a*] F. Cardano,[a] C. Barolo,[a,b,c] G. Viscardi,[a,b] A. Fin[a]

[a] Department of Chemistry, NIS Interdepartmental Centre and INSTM Reference Centre, University of Turin, Via P. Giuria 7, 10125, Torino, Italy
[b] ICxT Interdepartmental Center, University of Turin, Lungo Dora Siena 100, 10153 Torino, Italy
[c] Istituto di Scienza, Tecnologia e Sostenibilità per lo Sviluppo dei Materiali Ceramici (ISSMC-CNR), Via Granarolo 64, 48018 Faenza (RA) Italia

Keywords: imidazo[5,1-*a*]isoquinoline, imidazo[1,5-*a*]pyridine, luminescence, fluorescence, large Stokes shift.

Abstract

A series of new emissive imidazo[5,1-*a*]isoquinolines were synthesized, and their electronic properties investigated, compared, and discussed in light of their chemical structure. The electronic spectra show absorption bands around 330-350 nm and intense fluorescence emissions between 440 nm and 460 nm, with corresponding huge Stokes shifts (6464-8611 cm^{-1}). Depending on the position and the electronic properties of the substituents on the imidazo[5,1-*a*]isoquinoline nucleus, the emission quantum yield in dichloromethane solution enhances from 9% to 37%. The collected data suggest that two distinct mechanisms are responsible for the enhanced emission: the steric hindering of the rotation of the substituent and its electronic effect, improved by the molecular planarization attainable exclusively with electron-withdrawing substituents in *para* position.

1. Introduction

Small fluorescent molecules are powerful tools employed in a plethora of practical applications and everyday products. Intense emission, as well as defined absorption, optical tunability, and significant Stokes shift (to avoid reabsorption), represent the most critical requirements for any luminescent scaffold designed for possible technological applications in the fields of lighting, down-converting, fluorescence, and confocal microscopy or any other field applying luminescent molecules [1–8].

In this context, the imidazopyridine skeleton, which consists of an imidazole moiety fused to a pyridine ring, represents an important biologically-active nitrogen-containing heterocycle and an intense and versatile fluorogenic nucleus. Among imidazopyridine derivatives, the most reported are: imidazo[1,5-*a*]pyridines [9–11], imidazo[1,2-*a*]pyridines [12–14], imidazo[5,1-*a*]quinolones [15–17] and imidazo[2,1-*a*]isoquinolines (Figure 1); being important classes of nitrogen ring-junction heterocyclic compounds for optical, technological and medical applications [9,18].

Due to synthetic difficulties, imidazo[5,1-*a*]isoquinoline is the least investigated imidazopyridine moiety, despite its promising optical properties and the extended π-system [19]. Recently, some procedures have been reported, underlining the importance of developing new synthetic approaches to collect this poorly investigated heterocyclic skeleton [19–21]. In this context, we propose here an easy synthetic strategy to obtain the 1,3-disubstituted imidazo[5,1-*a*]isoquinoline nucleus (Figure 1) starting from substituted aromatic aldehydes and the well-known alkaloid papaverine. The reaction conditions are similar to those previously reported to synthesize related imidazo[1,5-*a*]pyridine derivatives [22,23].

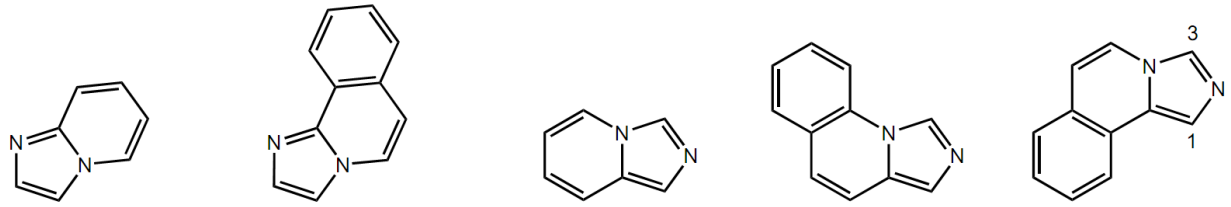

Figure 1. Chemical structures of the principally investigated imidazopyridine and imidazoquinoline skeletons.

Among the different families of luminophores, the imidazopyridine core has been widely studied due to its intense emission combined with a large Stokes shift [24–29]. Moreover, the electroluminescence of different imidazopyridines and imidazoquinoline has been recently investigated to develop layered OLEDs based on these fluorogenic nuclei showing promising performances [16,17,30–33]. In this context, a few previous works highlight a close relationship between optical properties and chemical modifications in different positions of the imidazopyridine skeleton, pointing out the importance of hindering the rotation of the substituents in positions 1 and 3 to increase the quantum yield [34–37].

Inspired by these notions, herein we present a study on an innovative synthetic approach to obtain five new fluorescent imidazo[5,1-*a*]isoquinolines (see molecular structures in Figure 2). The molecules are designed to investigate the relationship between the chemical structure (position of electron-donating or electron-withdrawing substituent groups) and the corresponding optical-electronic behaviour to pave the way, for this class of low-cost fluorophores, to technological applications in devices or as free emitters in sensors or fluorescence microscopy, as recently reported for these versatile fluorogenic nuclei [19,21,38–43].

The main target of this work is to investigate the relation between the position and the electronic nature of inserted substituent groups and the optical behaviour of the resulting emitters. In particular, to further improve the emissive features, we adopted two different strategies: i) the introduction of substituent groups (on the phenyl in position 1) in *ortho* and *para* position to exploit the rotational barrier as previously reported by us on similar imidazo[1,5-*a*]pyridine emitters; ii) the introduction of electron-donating or electron-withdrawing substituents to evaluate the specific electronic role of these groups on the electron-rich imidazo[5,1-*a*]isoquinoline scaffold.

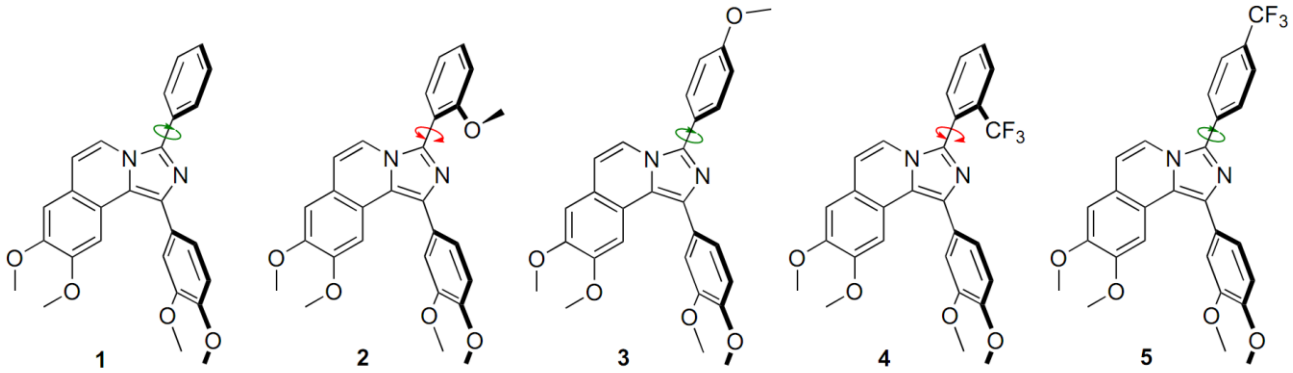

Figure 2. Chemical structures of the studied imidazo[5,1-*a*]isoquinolines.

2. Results and discussion

2.1. Synthesis

The novel compounds **1**–**5** are based on the luminescent imidazo[5,1-*a*]isoquinoline skeleton and were obtained applying a synthetic approach previously developed to obtain the imidazo[1,5-*a*]pyridine nucleus [23,44]. Specifically, the reaction consists in the condensation of (6,7-dimethoxyisoquinolin-1-yl)(3,4-dimethoxyphenyl)methanone (commonly known as "papaveraldine") with differently substituted aromatic aldehydes. Compound **1** was obtained using benzaldehyde, compounds **2** and **3** using 2-methoxybenzaldehyde and 4-methoxybenzaldehyde, respectively. Similarly, compounds **4** and **5** were obtained using 2-trifluoromethyl benzaldehyde and 4-trifluoromethyl benzaldehyde, respectively.

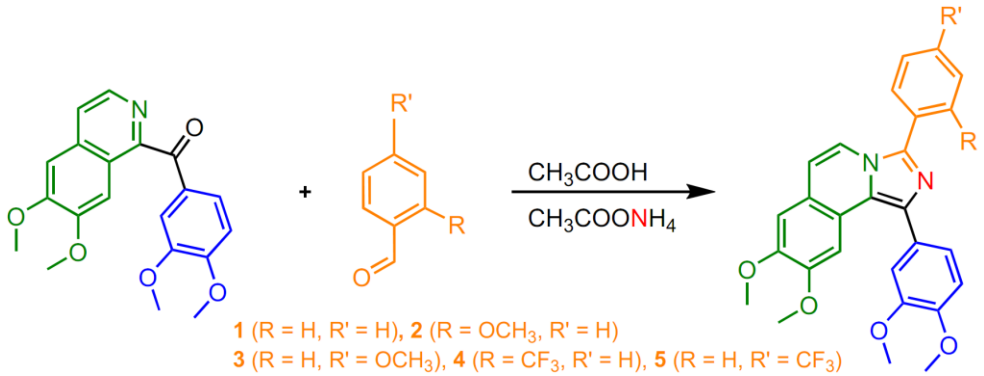

Scheme 1. Condensation reaction to obtain imidazo[5,1-*a*]isoquinolines **1**–**5**.

The papaveraldine was synthesised in high yield oxidizing the papaverine in mild conditions, as previously reported [45]. Papaverine is a well-known antispasmodic drug collected by extraction from *Papaver somniferum* (L., 1753). Here, it has been employed as a valuable precursor to obtain a

suitable ketone for the successive heterocyclization; this is particularly remarkable given the difficulty of finding on the market (or synthesizing) such kind of key reagents.
Compound **1** was selected as a reference for this study due to the absence of chemical groups on the phenyl ring in position 3 on the imidazo[5,1-*a*]isoquinoline, and the presence of the intact veratrole unit in position 1. Indeed, employing the papaveraldine as a ketone reagent, the obtained derivatives maintain the veratrole unit in position 1 on the imidazo[5,1-*a*]isoquinoline nucleus.
Since imidazo[5,1-*a*]isoquinoline is an electron-rich nucleus, we planned to investigate the effect of both electron-donating (methoxy) and electron-withdrawing (trifluoromethyl) groups, adequately introduced in *ortho* and *para* positions on the phenyl in position 3.
The synthetic approach is extremely promising, especially when compared to the previously reported strategies, which involve the use of either toxic or expensive catalysts such as SeO_2 [21] or $PdCl_2$ [46]. Recently imidazo[5,1-*a*]isoquinolines have been obtained by direct reaction of isoquinolin-1-yl(phenyl)methanone and 2-formylbenzoic acid in acid conditions [38]. Unfortunately, this last approach is severely limited by the commercial availability of alternative ketones suitable to obtain the target imidazo[5,1-*a*]isoquinoline skeleton. For these reasons, using papaveraldine ketone, derived from highly available and inexpensive papaverine, is an excellent choice for designing 3-substituted imidazo[5,1-*a*]isoquinoline emitters.

2.2 Photophysical characterization

The absorption and emission spectra of compounds **1**–**5** in dichloromethane solution are shown in Figure 3, and a selection of their photophysical data is reported in Table 1.
All the compounds are characterized by a main absorption band at $\lambda_{max} \sim$ 330-350, with almost no absorption beyond 440 nm. The molecules have a moderate molar absorption coefficient, log(**ε**) ~4. From this point of view, introducing the methoxy or the trifluoromethyl group in different positions of the 1,3-substituted-imidazo[1,5-*a*]pyridine nucleus does not cause any appreciable shift in the absorbance maxima in comparison to compound **1** (see Table 1). Only compound **5** differs slightly, showing a peculiar bathochromic shift (see Figure 3).

Table 1. Selected photophysical properties of compound **1**–**5** in dichloromethane solution.

Compound	λ_{abs} (nm)	λ_{em} (nm)	Stokes shift (cm^{-1})	log ε ($M^{-1}cm^{-1}$)	Φ	Lifetime (ns)	k_r (10^9 s^{-1})	k_{nr} (10^9 s^{-1})
1	333	453	7955	4.22	0.10	3.7	0.03	0.24
2	341	445	6854	4.17	0.19	5.0	0.04	0.16
3	330	461	8611	4.19	0.09	3.8	0.02	0.24
4	336	454	7735	4.21	0.22	3.0	0.07	0.26
5	351	454	6464	4.27	0.37	1.8	0.21	0.35

$k_r = \varphi/\tau$ and $k_{nr} = (1-\varphi)/\tau$

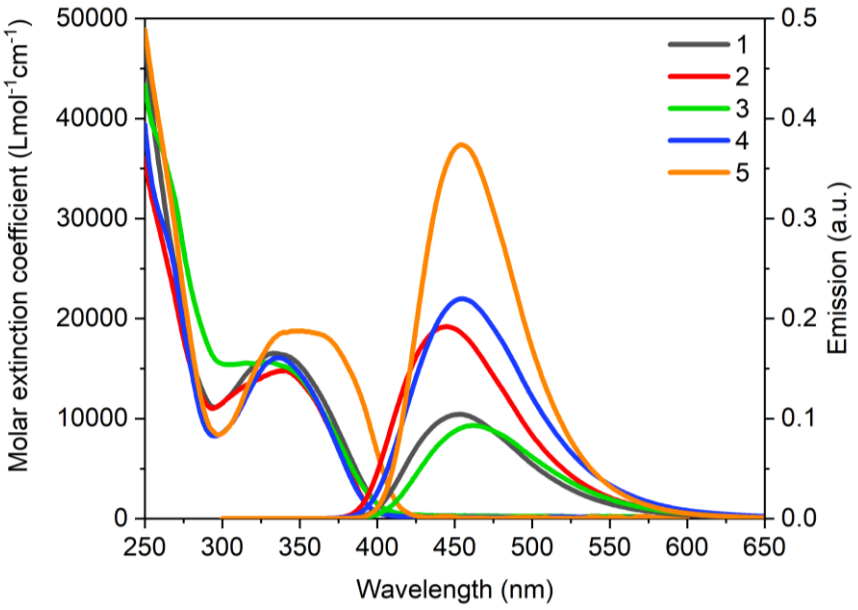

Figure 3. Absorption and emission spectra of compounds **1**–**5** in dichloromethane solution.

All the studied products exhibit an intense emission in the blue region, consistent with previous findings on similar heterocycles [16,17,19,21,27,38,47–49]. In detail, the fluorescence pick of these molecules is centred at λ_{max}~450-460 nm, with emission quantum yields ranging from 9% (compound **3**) to 37% (compound **5**). These values are comparable to the best results reported in the literature for other imidazopyridine derivatives [50–56]. However, the quantum yield is strongly influenced by both nature and position of the substituent employed. Indeed, the synthetic strategies adopted to design **1**–**5** led to a small shift of the emission, related to a significant modification of the quantum yield.

In this series, the veratrole unit in position 1 (the 1,2-dimethoxybenzene unit derived from the papaverine reagent) is present in every prepared compound, as well as the two methoxy substituent on the imidazo[5,1-*a*]isoquinoline nucleus, both deriving from the papaverine structure. Thus, any differences in the optical properties must be attributed to the designed substituent on the phenyl in position 3 of the heterocyclic nucleus. In the design of fluorophores **1**–**5**, we focused on introducing electron-donating (methoxy) and electron-withdrawing (trifluoromethyl) groups, employing adequate aldehydes for the heterocyclization.

As previously reported, the methoxy substituent is considered one of the most efficient groups to increase the fluorescence of imidazo[1,5-a]pyridines, mainly when introduced in the *ortho* position [23,50,57,58]. Compound **2** shows a higher quantum yield than **1** and **3**, confirming the substituent's fundamental structural role in hindering the rotation of the phenyl in 3 on the imidazo[5,1-*a*]isoquinoline. Conversely, the methoxy introduced in *para* position (product **3**) leads to a quantum emission yield comparable to that of the unsubstituted compound **1**; this result is related to the free rotation of the phenyl ring in compounds **1** and **3**. Thus, the differences in the optical behaviour of **1**–**3** are attributable to the rotational block, while no modifications in the character of the electronic transition are observable. The values of the radiative (k_r) and non-radiative (k_{nr}) rate constants are in agreement with this picture; indeed, k_r is the same for **1**–**3**, while k_{nr} decreases in the case of the *ortho* substituted molecule (**2**), as a consequence of the rotation hindrance.

Conversely, introducing an electron-withdrawing group (trifluoromethyl) in *ortho* and *para* positions produces a different situation, with a significant increase of both k_r and k_{nr}. The rotational block can

still be considered the main influencing factor for compound **4**, bearing an electron-withdrawing group (trifluoromethyl) in the *ortho* position. Indeed, the steric effect of this substituent is superior to the corresponding methoxy group of **2** (A-values of 2.4 ad 0.65 kcal/mol, respectively). Thus, the steric role of the substituent in the *ortho* position in hindering the rotation of the substituted phenyl in position 3 is confirmed, and the corresponding quantum yield is comparable (19% and 22% for **2** and **4**, respectively). Conversely, compound **5** shows a further increase in quantum yield that must be attributed to a different factor. In this case, the suitable planarization of the molecule plays a key role in obtaining an effective push-pull system driven by the presence of the electron-withdrawing group (trifluoromethyl) in the *para* position. The crucial role of planarization in increasing the push-pull effect and achieving high quantum yield has been widely reported also for other emitting systems.[59–61] In our case, this leads compound **5** to the best optical performance, with a significant increase in quantum yield, which is four times higher when compared with **1** and **3**, and double when compared with **2** and **4**. These optical performances are comparable with those of well-known commercial emitters such as: 4-Methylumbelliferone (λ_{abs}~ 360 nm, λ_{em}~ 450 nm, log ε=4.23, Φ=0.63), Alexa Fluor 350 (λ_{abs}~ 346 nm, λ_{em}~ 442 nm, log ε=4.28), Hoechst 33342 (λ_{abs}~ 350 nm, λ_{em}~ 461 nm, log ε=4.65, Φ=0. 0.38), ECFP (λ_{abs}~ 434 nm, λ_{em}~ 477 nm, log ε=4.41, Φ=0.4) [62,63]. Solvatochromic studies support the correlations between chemical structure and optical behaviour outlined above (see Figure 4 and Figures S16-20). The emission spectra of all the reported compounds **1–5** are characterized by well-defined peaks in all solvents. On the other hand, in agreement with calculated values, the ground state absorption is depicted by broad bands for compounds **1**, **3**, and **5**. In contrast, compounds **2** and **4**, most likely due to the presence of the substituent in the *ortho* position that hampers the planarization, are depicted by better-defined peaks. As a function of a solvent polarity parameter ET(30), the Stokes shift analysis in various solvents highlights very weak sensitivity to polarity for the unsubstituted **1** and compounds **2** and **4**, most likely due to less efficient planarization due to *ortho* substituents. On the other hand, compounds **3** and **5** are more sensitive to solvent polarity, but in a divergent way, as expected considering the presence in *para* of an electron-donating or an electron-withdrawing group, respectively.

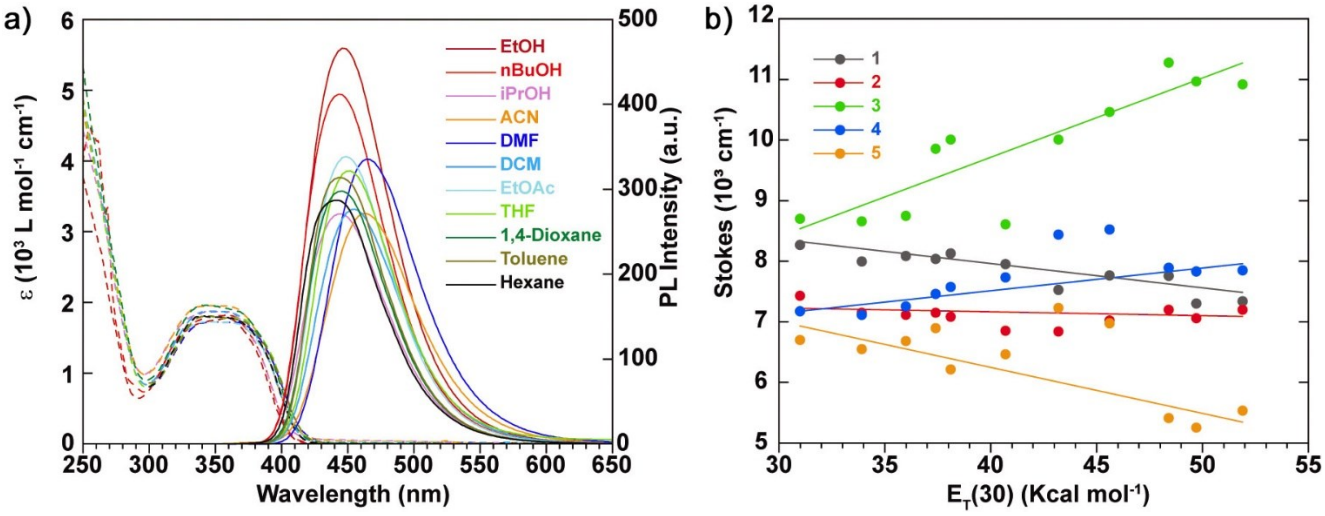

Figure 4. (a) Absorption (dashed line) and emission (solid line) spectra of **5** in different solvents. (b) Polarity plot of the Stokes shift as a function of solvent polarity parameter $E_T(30)$.

2.3 Theoretical calculations

To gain insight into the scenario of electronic excited states involved in the photophysics of **1**–**5**, DFT and TD-DFT calculations were performed.

In detail, for **1**–**3**, the electron density redistribution upon the lowest electronic transition (tr. 1) highlights the π→π* nature of the first singlet excited state (S1), deriving from a π→π* excitation centred on the imidazo[5,1-*a*]isoquinoline portion of the molecule, albeit with a contribution of electronic density donated by the veratrole unit in position 1 (see electron-density difference maps EDDMs and orbital composition Figure 5, Figure S21 and Tables S1-S4).

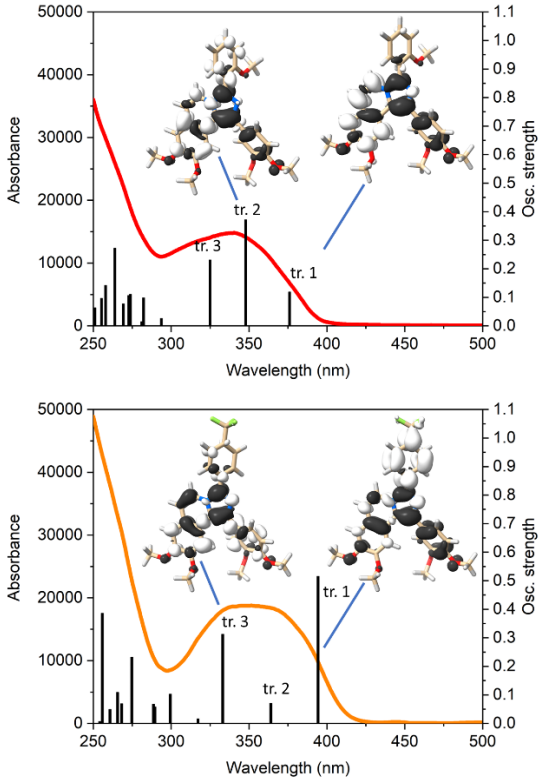

Figure 5. Experimental electronic absorption spectra of **2** (top, red curve) and **5** (bottom, orange curve) in dichloromethane solution, together with calculated singlet excited state transitions (vertical bars with height equal to the oscillator strength values). EDDMs of selected electronic transitions (black indicates a decrease in electron density, and white indicates an increase).

In the case of compounds **4** and **5**, the role of the electron-withdrawing trifluoromethyl group becomes evident. Indeed, the phenyl in position 3 on the imidazo[5,1-*a*]isoquinolines nucleus is involved in the lowest electronic transition (tr. 1), accepting electronic density. The phenomenon is particularly evident in the case of **5**, for which the bathochromic shift of the absorption band can be assigned to the predominant contribution of tr. 1, showing an electronic density displacement from the veratrole portion toward the electron-withdrawing trifluoromethyl group (see electron-density difference maps and orbital composition in Table S5-6, Figure 5 and Figure S21).

To substantiate this point, the geometry of the corresponding singlet excited state (S_1) has been optimized and compared with the ground state (S_0). Table 2 collects the dihedral angles α_1 and α_2 that have been identified as the most convenient to evaluate the planarization of the excited state. As can be seen from these computational data, the structures of compounds **1**, **3,** and **5** in their electronic

excited state (S_1) show a marked planarization with respect to the ground state (S_0). The push-pull effect is precluded in the case of compound **4**, where the *ortho*-substituted CF_3 group while attracting electronic density, hinders the planarization. Likewise, the same transition (tr. 1) is present also in the absorption of compound **4** but falls at a shorter wavelength and is characterized by a lower oscillator strength.

Table 2. Calculated dihedral angles α_1 and α_2 in the ground and excited states of **1**–**5** in dichloromethane solution.

	State	$\alpha_{1(N2\text{-}C3\text{-}C4\text{-}C5)}$ (°)	$\alpha_{2(N2\text{-}C1\text{-}C6\text{-}C7)}$ (°)
1 (R = H, R' = H)	S_0	35.3	42.7
	S_1	23.5	27.6
2 (R = OCH_3, R' = H)	S_0	57.6	42.9
	S_1	42.0	28.0
3 (R = H, R' = OCH_3)	S_0	35.8	42.3
	S_1	21.0	29.1
4 (R = CF_3, R' = H)	S_0	57.5	43.7
	S_1	42.2	25.0
5 (R = H, R' = CF_3)	S_0	33.2	43.3
	S_1	21.9	26.3

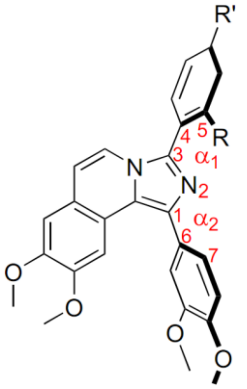

Summarizing, the analysis of the optical properties of compounds **1**–**5** suggests that two different and fundamental roles must be evoked to justify the increase of the optical behaviours: the structural role of the substituent in *ortho* position in hindering the rotation of the phenyl in position 3 (as previously demonstrated by us on similar heterocyclic emitters) and the electronic role of the electron-withdrawing group able to generate a push-pull effect in the excited state (allowed by the planarization of the emitter). These two essential requisites are simultaneously satisfied only in the case of compound **5**.

2.4 Electrochemical characterization

The electrochemical properties of a new fluorophore are paramount for any technological application. For example, the absolute energy-level position of frontier orbital is a fundamental information for the choice of electro-active materials to effectively inject charge carriers into thin films of organic molecules or act as hole-transporting materials.

Table 3 summarizes the redox processes of compounds **1**–**5**, analyzed by cyclic voltammetry in dichloromethane solution (3 mM), while Figure 6 compares the value of the first oxidation peak along the series. All the studied compounds display multiple mono-electronic oxidations (except **4,** which shows a single irreversible oxidation).

Table 3. Redox potentials (vs. Ag/Ag^+ reference) of compounds **1**–**5** in dichloromethane solution (3 mM).

	Oxidation	Reduction
1	$E_{1/2} = 0.81$, $E_{1/2} = 1.25$	$E_{irr} = -1.89$
2	$E_{1/2} = 0.79$, E = 1.28, E = 1.34	$E_{irr} = -1.79$
3	$E_{1/2} = 0.76$, E = 1.25, E = 1.33	$E_{irr} = -1.72$
4	$E_{irr} = 0.98$	$E_{irr} = -1.83$
5	$E_{1/2} = 0.88$, E = 1.32, E = 1.40	$E_{irr} = -1.80$

Albrecht et Al. previously investigated the electrochemistry behaviors of similar 1,3-disubstituted imidazo[1,5-*a*]quinolines reporting that their compounds *"in this study do not show chemical reversibility in their oxidation waves"* [47] at the contrary the products here reported show complete reversibility at the first oxidation step. Similarly, a large number of imidazo[1,5-*a*]pyridines have been reported confirming reversible oxidation at about 600-800 mV (vs. Ag/Ag^+) centered on the electron-rich heterocyclic nucleus [16,17,30,34,47,64–66].

The first oxidation of compounds **1**–**5** is characterized by a potential of about 800 mV (vs. Ag/Ag^+). In the case of compounds **1**–**3** and **5**, this oxidation is reversible (see Figure 6), while in the case of compound **4**, it is also irreversible at a high scan rate (until 800 mV/s). The peculiar irreversibility of compound **4** remembers the cyclic voltammetry reported by Albrecht et al. l. for 3-fluorophenyl-imidazo[1,5-*a*]quinoline. It could be caused by a chemical reaction that removes the oxidized molecules from the electrode surface and thereby hinders the reduction [47].

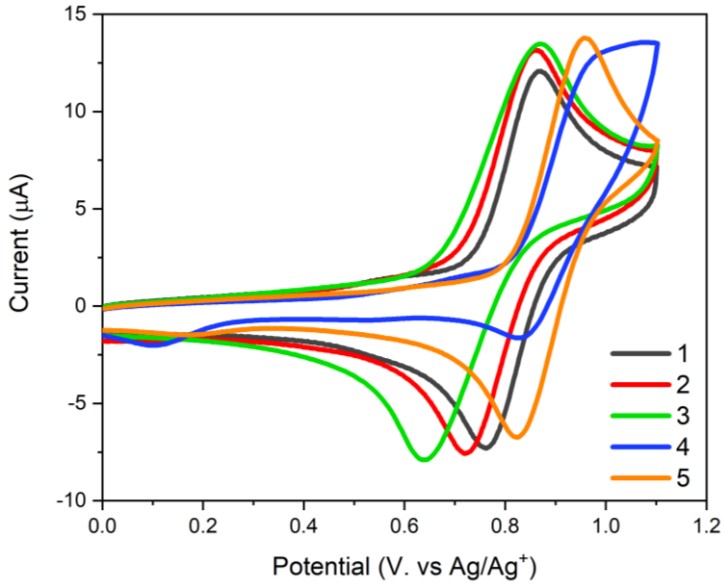

Figure 6. Cyclic voltammetry: first oxidation process of compounds **1**–**5** in dichloromethane solution (3 mM).

In general, the methoxylated compounds **2** and **3** are oxidized at less-positive potentials when compared to compound **1**, attesting to the significant electron-donating effect of the methoxy substituent on the imidazo[5,1-*a*]isoquinoline nucleus in different positions. On the contrary, the trifluoromethylated compounds **4** and **5** are oxidized at higher values, demonstrating the opposite role of the electron-withdrawing inserted functional group independently by its position (*ortho* or *para*). A similar trend can be observed for the second oxidation (if present) and the reduction process (at about –1.80 V for all the products, see Table 3).

3. Experimental details

3.1 Materials and Techniques

All solvents and raw materials were used as received from commercial suppliers (Sigma-Aldrich and Alfa Aesar) without further purification.

TLC was performed on Fluka silica gel TLC-PET foils GF 254, particle size 25 nm, medium pore diameter 60 Å. Column chromatography was performed on Sigma-Aldrich silica gel 60 (70-230 mesh ASTM).
^{1}H and ^{13}C NMR spectra were recorded on a JEOL JNM-ECZR 600 spectrometer (^{1}H NMR operating frequency 600 MHz). Chemical shifts are reported relative to TMS ($\delta = 0$) and referenced against solvent residual peaks. The following abbreviations are used: s (singlet), d (doublet), t (triplet), dd (doublet of doublets), m (multiplet).
ESI-HRMS electrospray ionization high-resolution mass experiments were obtained with a Thermo Orbitrap Fusion mass spectrometer.
UV-Vis absorption spectra were recorded on a Cary60 spectrometer. Photoemission spectra, luminescence lifetimes, and quantum yields were acquired with a HORIBA Jobin Yvon IBH Fluorolog-TCSPC spectrofluorometer equipped with a Quanta-φ integrating sphere.
Cyclic voltammetry experiments were performed using a Metrohm Autolab 302 N potentiostat. The electrochemical cell was a single-compartment cell equipped with a standard three-electrode set-up: a glassy carbon working electrode (Ø = 1 mm), a Pt-wire counter electrode, and an Ag/AgCl (KCl 3 M) reference electrode. All measurements were carried out in dichloromethane with tetrabutylammonium hexafluorophosphate 0.1 M as the supporting electrolyte.

3.2 Syntheses

(6,7-dimethoxyisoquinolin-1-yl)(3,4-dimethoxyphenyl)methanone has been obtained, as previously reported, by direct oxidation of papaverine reagent in mild conditions [45]. This ketone was employed with differently substituted aldehydes for a successive one-pot heterocyclization to obtain the imidazo[5,1-*a*]isoquinoline derivatives employing a previously reported procedure to synthesize imidazo[1,5-*a*]pyridine products [23,26,52,67,67–70].
General procedure for compounds **1**–**5**:
A mixture of (6,7-dimethoxyisoquinolin-1-yl)(3,4-dimethoxyphenyl)methanone (150 mg, 0.42 mmol), substituted benzaldehyde (0.63 mmol), ammonium acetate (160 mg, 2.1 mmol) and 10 ml of acetic acid was refluxed overnight. After, the reaction mixture was cooled to 80 °C, and the acetic acid was removed by vacuum distillation. The resulting solid was dissolved in a saturated aqueous sodium carbonate solution, and the mixture was extracted with dichloromethane. The organic layer was separated and dried over sodium sulphate, and the solvent was evaporated under a vacuum. The desired product was purified by flash chromatography on silica gel using dichloromethane/methanol (99:1).

1-(3,4-dimethoxyphenyl)-8,9-dimethoxy-3-phenylimidazo[5,1-*a*]isoquinoline (**1**)
The product was isolated as a yellow powder (120 mg, 65%). R_f (silica gel): 0.25 (95:5 dichloromethane/methanol). ^{1}H-NMR (600 MHz, $CDCl_3$, RT): δ 7.98-7.99 (d, J = 7.4 Hz, 1H, Ar-H), 7.83-7.85 (m, 2H, Ar-H), 7.52-7.56 (m, 3H, Ar-H), 7.45-7.47 (tt, J = 7.4 Hz, J = 1.9 Hz, 1H, Ar-H), 7.34-7.36 (dd, J = 8.1 Hz, J = 2.0 Hz, 1H, Ar-H), 7.31 (d, J = 2.0 Hz, 1H, Ar-H), 7.01-7.02 (d, J = 8.2 Hz, 1H, Ar-H), 6.99 (s, 1H, Ar-H), 6.72-6.73 (d, J = 7.5 Hz, 1H, Ar-H), 3.96 (s, 3H, -CH_3), 3.95 (s, 3H, -CH_3), 3.92 (s, 3H, -CH_3), 3.65 (s, 3H, -CH_3) ppm. ^{13}C-NMR (151 MHz, $CDCl_3$, RT): δ 149.55, 149.11, 148.87, 139.41, 133.63, 130.24, 129.24, 129.17, 129.09, 128.84, 128.36, 125.43, 124.24, 122.67, 121.95, 119.97, 119.31, 113.69, 113.45, 111.17, 108.25, 104.85, 56.22, 56.11, 56.09, 55.88 ppm. MS (ESI^+, MeOH): m/z 441.1843 $[M+H]^+$; calculated for $C_{27}H_{24}N_2O_4$: 441.1809 (+1).

1-(3,4-dimethoxyphenyl)-8,9-dimethoxy-3-(2-methoxyphenyl)imidazo[5,1-*a*]isoquinoline (**2**)

The product was isolated as a yellow powder (118 mg, 61%). R_f (silica gel): 0.40 (95:5 dichloromethane/methanol). ^{1}H-NMR (600 MHz, $CDCl_3$, RT): δ 7.68-7.70 (dd, *J* = 7.5 Hz, *J* = 1.4 Hz, 1H, Ar-H), 7.62 (s, 1H, Ar-H), 7.47-7.50 (m, 1H, Ar-H), 7.37-7.40 (m, 2H, Ar-H), 7.35 (d, *J* = 1.9 Hz, 1H, Ar-H), 7.11-7.13 (td, *J* = 7.5 Hz, *J* = 1.1 Hz, 1H, Ar-H), 7,05-7,06 (d, *J* = 8.3 Hz, 1H, Ar-H), 6.99-7.01 (m, 2H, Ar-H), 3.96 (s, 3H, -CH_3), 3.95 (s, 3H, -CH_3), 3.92 (s, 3H, -CH_3), 3.83 (s, 3H, -CH_3), 3.67 (s, 3H, -CH_3) ppm. ^{13}C-NMR (151 MHz, $CDCl_3$, RT): δ 157.61, 149.25, 149.01, 148.71, 148.67, 137.27, 133.36, 133.06, 131.06, 129.50, 123.82, 122.63, 121.99, 121.29, 120.79, 119.89, 113.49, 112.47, 111.24, 111.03, 108.15, 104.81, 56.17, 56.08, 56.05, 55.90, 55.68 ppm. MS (ESI^+, MeOH): m/z 471.1949 $[M+H]^+$; calculated for $C_{28}H_{26}N_2O_5$: 471.1914 (+1).

1-(3,4-dimethoxyphenyl)-8,9-dimethoxy-3-(4-methoxyphenyl)imidazo[5,1-*a*]isoquinoline (**3**)
The product was isolated as a yellow powder (122 mg, 63%). R_f (silica gel): 0.30 (95:5 dichloromethane/methanol). ^{1}H-NMR (600 MHz, $CDCl_3$, RT): δ 7.91-7.92 (d, *J* = 7.4 Hz, 1H, Ar-H), 7.75-7.77 (m, 2H, Ar-H), 7.55 (s, 1H, Ar-H), 7.34-7.35 (dd, *J* = 8.2 Hz, *J* = 1.9 Hz, 1H, Ar-H), 7.31 (d, *J* = 1.8 Hz, 1H, Ar-H), 7.05-7.07 (m, 2H, Ar-H), 7.00-7.01 (d, *J* = 8.2 Hz, 1H, Ar-H), 6.98 (s, 1H, Ar-H), 6.70-6.71 (d, *J* = 7.4 Hz, 1H, Ar-H), 3.96 (s, 3H, -CH_3), 3.95 (s, 3H, -CH_3), 3.92 (s, 3H, -CH_3), 3.89 (s, 3H, -CH_3), 3.65 (s, 3H, -CH_3) ppm. ^{13}C-NMR (151 MHz, $CDCl_3$, RT): δ 160.31, 149.50, 149.09, 148.83, 148.78, 139.36, 133.20, 130.30, 129.18, 128.38, 123.87, 122.66, 121.86, 120.00, 119.34, 114.54, 113.55, 113.43, 111.14, 108.26, 104.80, 56.21, 56.10, 56.08, 55.88, 55.55 ppm. MS (ESI^+, MeOH): m/z 471.1948 $[M+H]^+$; calculated for $C_{28}H_{26}N_2O_5$: 471.1914 (+1).

1-(3,4-dimethoxyphenyl)-8,9-dimethoxy-3-(2-(trifluoromethyl)phenyl)imidazo[5,1-*a*]isoquinoline (**4**)
The product was isolated as a yellow powder (79 mg, 37%). R_f (silica gel): 0.40 (95:5 dichloromethane/methanol). ^{1}H-NMR (600 MHz, $CDCl_3$, RT): δ 7.87-7.88 (d, *J* = 7.7 Hz, 1H, Ar-H), 7.70-7.73 (t, *J* = 7.5 Hz, 1H, Ar-H), 7.65-7.68 (m, 3H, Ar-H), 7.37-7.39 (dd, *J* = 8.1 Hz, *J* = 1.9 Hz, 1H, Ar-H), 7.34 (d, *J* = 1.7 Hz, 1H, Ar-H), 7.27-7.29 (d, *J* = 7.4 Hz, 1H, Ar-H), 6.99-7.01 (m, 2H, Ar-H), 6.68-6.69 (d, *J* = 7.3 Hz, 1H, Ar-H), 3.94-3.96 (m, 9H, -CH_3), 3.69 (s, 3H, -CH_3) ppm. ^{13}C-NMR (151 MHz, $CDCl_3$, RT): δ 149.61, 149.06, 148.97, 148.83, 135.56, 133.30, 132.15, 131.44, 131.24, 130.23, 129.05, 127.08, 124.64, 123.52, 122.82, 122.56, 121.91, 119.62, 119.07, 113.61, 113.38, 110.99, 108.37, 104.87, 56.18, 56.10, 56.08, 55.96 ppm. MS (ESI^+, MeOH): m/z 509.1715 $[M+H]^+$; calculated for $C_{28}H_{23}F_3N_2O_4$: 509.1683 (+1).

1-(3,4-dimethoxyphenyl)-8,9-dimethoxy-3-(4-(trifluoromethyl)phenyl)imidazo[5,1-*a*]isoquinoline (**5**)
The product was isolated as a yellow powder (145 mg, 68%). R_f (silica gel): 0.50 (95:5 dichloromethane/methanol). ^{1}H-NMR (600 MHz, $CDCl_3$, RT): δ 7.99-8.00 (m, 3H, Ar-H), 7.78-7.80 (d, *J* = 8.2 Hz, 2H, Ar-H), 7.55 (s, 1H, Ar-H), 7.32-7.34 (dd, *J* = 8.1 Hz, *J* = 2.0 Hz, 1H, Ar-H), 7.29 (d, *J* = 1.9 Hz, 1H, Ar-H), 7.01-7.03 (m, 2H, Ar-H), 6.79-6.81 (d, *J* = 7.5 Hz, 1H, Ar-H), 3.95-3.97 (m, 6H, -CH_3), 3.92 (s, 3H, -CH_3), 3.65 (s, 3H, -CH_3) ppm. ^{13}C-NMR (151 MHz, $CDCl_3$, RT): δ 149.77, 149.19, 149.14, 149.04, 137.72, 134.28, 133.77, 130.75, 130.53, 128.90, 128.81, 126.09, 126.07, 125.00, 123.25, 122.67, 122.01, 119.84, 118.81, 114.40, 113.37, 111.22, 108.24, 104.86, 56.23, 56.11, 55.90 ppm. MS (ESI^+, MeOH): m/z 509.1716 $[M+H]^+$; calculated for $C_{28}H_{23}F_3N_2O_4$: 509.1683 (+1).

3.3 Calculations

All calculations were performed with the Gaussian 16 program package [71], employing the Density Functional Theory (DFT) and its Time-Dependent extension TD-DFT [72,73]. The Becke's three-parameter hybrid functional [74] and the Lee-Yang-Parr's gradient corrected correlation functional (B3LYP) [75] were used together with the 6-31G** basis set [76]. The solvent effect was included using the polarizable continuum model (CPCM method) [77,78], with dichloromethane as the solvent. Geometry optimizations were carried out for ground (S_0) and first electronic excited (S_1) states without any symmetry constraints. The nature of all stationary points was verified via harmonic vibrational frequency calculations, and no imaginary frequencies were found, indicating we had located minima on potential energy surfaces. Electronic transitions were computed from S_0 as vertical excitation with linear response solvation by TD-DFT [72,73], employing the ground state optimized geometries. A total of 128 singlet excited states was computed for each compound, and the electronic distribution and the localization of the singlet excited states were visualized using Electron Density Difference Maps. GaussSum 2.2.5 [79] was used to simulate the theoretical UV-Vis spectra and for EDDMs calculations [80,81]. Molecular-graphic images were produced by using the UCSF Chimera package from the Resource for Biocomputing, Visualization, and Informatics at the University of California, San Francisco [82].

4. Conclusions

Five new imidazo[5,1-*a*]isoquinolines derivatives have been designed to improve the optical performances of this promising but poorly studied luminescent nucleus, belonging to the widely investigated class of imidazopyridine emitters. The adopted synthetic strategy is innovative because it employs the well-known alkaloid papaverine as a source of suitable ketone for the direct one-pot heterocyclization. This approach represents a convenient alternative to using expensive and hardly achievable ketones required for this peculiar class of emitters.

The new luminescent imidazo[5,1-*a*]isoquinolines have been successfully substituted in different positions with both electron-donating (methoxy group) and electron-withdrawing groups (trifluoromethyl group) in *ortho* and *para* positions on the fluorogenic nucleus, tuning the corresponding optical and electrochemical properties.

The electronic absorption and emission properties have been investigated experimentally and computationally and rationalized to clarify the correlations between chemical structure and optical behaviour. All the compounds show an absorption maximum in the UV region without significant absorption in the visible range ($\lambda_{max} > 420$ nm), with a useful transparency in the visible range for possible applications in down shift technology. The studied imidazo[5,1-*a*]isoquinolines show intense emissions in the spectral range between 400 and 550 nm with large Stokes shifts of ~6500 to ~8600 cm^{-1}.

The introduction of electron-donating and electron-withdrawing groups in different positions on the imidazo[5,1-*a*]isoquinolines skeleton slightly modifies the absorption and emission range but highly enhances the photoluminescence quantum yield. The comparison of the optical properties along the series emphasizes the importance of the substitution in position 3, due to different reasons. As a matter of fact, the emission properties of compounds **2**, **4** and **5** show a strong increase (more than doubled) of the quantum yield with respect to compounds **1** and **2**.

The main contribution of this work is to identify two complemental key roles (steric and electronic) of the nature and position of the introduced substituents in tuning the optical properties: 1) the rotational hindering of the substituent group in position 3 on the imidazo[5,1-*a*]isoquinoline skeleton in increasing the emission quantum yield and 2) the strong electronic effect driven by electron-

withdrawing group (trifluoromethyl group) allowed by planarization of the emitters. These two key requisites justify the peculiar trend of the optical performances along the series.
In conclusion, the reported imidazo[5,1-*a*]isoquinolines show good or better electronic properties in comparison to the other widely reported imidazopyridines such as imidazo[1,5-*a*]pyridine and imidazo[1,2-*a*]pyridine, comparable with those of well-known commercial emitters [62,63]. For this reason, this work represents a clear insight for the design of new emissive molecules towards the application in lighting devices, down-converting technologies, fluorescence microscopy and other technological fields in which new emitters are strongly required.

Acknowledgments

Authors acknowledge support from the Project CH4.0 under the MUR program "Dipartimenti di Eccellenza 2023-2027" (CUP: D13C22003520001).

References

[1] Duan L, Hou L, Lee T-W, Qiao J, Zhang D, Dong G, et al. Solution processable small molecules for organic light-emitting diodes. J Mater Chem 2010;20:6392–407. https://doi.org/10.1039/B926348A.
[2] Fresta E, Costa RD. Beyond traditional light-emitting electrochemical cells – a review of new device designs and emitters. J Mater Chem C 2017;5:5643–75. https://doi.org/10.1039/C7TC00202E.
[3] Huang T, Jiang W, Duan L. Recent progress in solution processable TADF materials for organic light-emitting diodes. J Mater Chem C 2018;6:5577–96. https://doi.org/10.1039/C8TC01139G.
[4] Niko Y, Konishi G. Molecular Design of Highly Fluorescent Dyes. J Synth Org Chem Jpn 2012;70:918–27. https://doi.org/10.5059/yukigoseikyokaishi.70.918.
[5] Wei Q, Fei N, Islam A, Lei T, Hong L, Peng R, et al. Small-Molecule Emitters with High Quantum Efficiency: Mechanisms, Structures, and Applications in OLED Devices. Adv Opt Mater 2018;6:1800512. https://doi.org/10.1002/adom.201800512.
[6] Hong Y, Lam JWY, Tang BZ. Aggregation-induced emission: phenomenon, mechanism and applications. Chem Commun 2009:4332. https://doi.org/10.1039/b904665h.
[7] He S, Song J, Qu J, Cheng Z. Crucial breakthrough of second near-infrared biological window fluorophores: design and synthesis toward multimodal imaging and theranostics. Chem Soc Rev 2018;47:4258–78. https://doi.org/10.1039/C8CS00234G.
[8] Sedgwick AC, Wu L, Han H-H, Bull SD, He X-P, James TD, et al. Excited-state intramolecular proton-transfer (ESIPT) based fluorescence sensors and imaging agents. Chem Soc Rev 2018;47:8842–80. https://doi.org/10.1039/C8CS00185E.
[9] Ramana Reddy M, Darapaneni CM, Patil RD, Kumari H. Recent synthetic methodologies for imidazo[1,5- *a*]pyridines and related heterocycles. Org Biomol Chem 2022:10.1039.D2OB00386D. https://doi.org/10.1039/D2OB00386D.
[10] Volpi G, Rabezzana R. Imidazo[1,5-a]pyridine derivatives: useful, luminescent and versatile scaffolds for different applications. New J Chem 2021. https://doi.org/10.1039/D1NJ00322D.
[11] Volpi G. Luminescent Imidazo[1,5- *a*]pyridine Scaffold: Synthetic Heterocyclization Strategies-Overview and Promising Applications. Asian J Org Chem 2022. https://doi.org/10.1002/ajoc.202200171.
[12] Zhang S, Yuan W, Qin Y, Zhang J, Lu N, Liu W, et al. Bidentate BODIPY-appended 2-pyridylimidazo[1,2-a]pyridine ligand and fabrication of luminescent transition metal complexes. Polyhedron 2018;148:22–31. https://doi.org/10.1016/j.poly.2018.03.023.
[13] Vanda D, Zajdel P, Soural M. Imidazopyridine-based selective and multifunctional ligands of biological targets associated with psychiatric and neurodegenerative diseases. Eur J Med Chem 2019;181:111569. https://doi.org/10.1016/j.ejmech.2019.111569.

[14] Mokhtari TS, Seifi M, Saheb V, Sheibani H. Polar [3+2] cycloaddition of isatin-3-imines with electrophilically activated heteroaromatic N-ylides: Synthesis of spirocyclic imidazo[1,2-a]pyridine and isoquinoline derivatives. Arab J Chem 2015. https://doi.org/10.1016/j.arabjc.2015.05.023.
[15] Wang H, Xu W, Xin L, Liu W, Wang Z, Xu K. Synthesis of 1,3-Disubstituted Imidazo[1,5-a]pyridines from Amino Acids via Catalytic Decarboxylative Intramolecular Cyclization. J Org Chem 2016;81:3681–7. https://doi.org/10.1021/acs.joc.6b00343.
[16] Albrecht G, Herr JM, Steinbach M, Yanagi H, Göttlich R, Schlettwein D. Synthesis, optical characterization and thin film preparation of 1-(pyridin-2-yl)-3-(quinolin-2-yl)imidazo[1,5-a]quinoline. Dyes Pigments 2018;158:334–41. https://doi.org/10.1016/j.dyepig.2018.05.056.
[17] Albrecht G, Geis C, Herr JM, Ruhl J, Göttlich R, Schlettwein D. Electroluminescence and contact formation of 1-(pyridin-2-yl)-3-(quinolin-2-yl)imidazo[1,5-a]quinoline thin films. Org Electron 2019;65:321–6. https://doi.org/10.1016/j.orgel.2018.11.032.
[18] Chitrakar R, Rawat D, Sistla R, Vadithe LN, Subbarayappa A. Design, synthesis and anticancer activity of sulfenylated imidazo-fused heterocycles. Bioorg Med Chem Lett 2021;49:128307. https://doi.org/10.1016/j.bmcl.2021.128307.
[19] Mahata S, Dey S, Mandal BB, Manivannan V. 3-(2-Hydroxyphenyl)imidazo[5, 1-a]isoquinoline as Cu(II) sensor, its Cu(II) complex for selective detection of CN− ion and biological compatibility. J Photochem Photobiol Chem 2022;427. https://doi.org/10.1016/j.jphotochem.2022.113795.
[20] Khalili G. A diastereoselective synthesis of (Z)-3-[(aryl)(hydroxyimino)methyl]-2-cyclohexyl-1-(cyclohexylamino)imidazo[5,1-a]isoquinolinium chlorides from isoquinoline, chlorooximes, and cyclohexyl isocyanide. Monatshefte Für Chem - Chem Mon 2016;147:429–33. https://doi.org/10.1007/s00706-015-1522-8.
[21] Bori J, Behera N, Mahata S, Manivannan V. Synthesis of Imidazo[5, 1-a]isoquinoline and Its 3-Substituted Analogues Including the Fluorescent 3-(1-Isoquinolinyl)imidazo[5, 1-a]isoquinoline. ChemistrySelect 2017;2:11727–31. https://doi.org/10.1002/slct.201702420.
[22] Wang J, Dyers L, Mason R, Amoyaw P, Bu XR. Highly efficient and direct heterocyclization of dipyridyl ketone to N,N-bidentate ligands. J Org Chem 2005;70:2353–6. https://doi.org/10.1021/jo047853k.
[23] Volpi G, Magnano G, Benesperi I, Saccone D, Priola E, Gianotti V, et al. One pot synthesis of low cost emitters with large Stokes' shift. Dyes Pigments 2017;137:152–64. https://doi.org/10.1016/j.dyepig.2016.09.056.
[24] Mohbiya DR, Sekar N. Tuning 'Stokes Shift' and ICT Character by Varying the Donor Group in Imidazo[1,5 a]pyridines: A Combined Optical, DFT, TD-DFT and NLO Approach. ChemistrySelect 2018;3:1635–44. https://doi.org/10.1002/slct.201702579.
[25] Hutt JT, Jo J, Olasz A, Chen C-H, Lee D, Aron ZD. Fluorescence Switching of Imidazo[1,5-a]pyridinium Ions: pH-Sensors with Dual Emission Pathways. Org Lett 2012;14:3162–5. https://doi.org/10.1021/ol3012524.
[26] Volpi G, Garino C, Priola E, Magistris C, Chierotti MR, Barolo C. Halogenated imidazo[1,5-a]pyridines: chemical structure and optical properties of a promising luminescent scaffold. Dyes Pigments 2019;171:107713. https://doi.org/10.1016/j.dyepig.2019.107713.
[27] Marchesi A, Brenna S, Ardizzoia GA. Synthesis and emissive properties of a series of tetrahydro (imidazo[1,5-a]pyrid-3-yl)phenols: a new class of large Stokes shift organic dyes. Dyes Pigments 2019;161:457–63. https://doi.org/10.1016/j.dyepig.2018.09.069.
[28] Priola E, Volpi G, Rabezzana R, Borfecchia E, Garino C, Benzi P, et al. Bridging Solution and Solid-State Chemistry of Dicyanoaurate: The Case Study of Zn–Au Nucleation Units. Inorg Chem 2020;59:203–13. https://doi.org/10.1021/acs.inorgchem.9b00961.
[29] Mandal A, Patel BK. Rationalization of weak interactions in two fluorescence active imidazo-[1,5-a]-pyridine derivatives: A combined experimental and computational study. J Mol Struct 2017;1147:735–46. https://doi.org/10.1016/j.molstruc.2017.07.08.
[30] Fresta E, Volpi G, Garino C, Barolo C, Costa RD. Contextualizing yellow light-emitting electrochemical cells based on a blue-emitting imidazo-pyridine emitter. Polyhedron 2018;140:129–37. https://doi.org/10.1016/j.poly.2017.11.048.

[31] Herr JM, Rössiger C, Locke H, Wilhelm M, Becker J, Heimbrodt W, et al. Synthesis, optical and theoretical characterization of heteroleptic Iridium(III) Imidazo[1,5-a]pyridine and -quinoline complexes. Dyes Pigments 2020;180:108512. https://doi.org/10.1016/j.dyepig.2020.108512.
[32] Cavinato LM, Volpi G, Fresta E, Garino C, Fin A, Barolo C. Microwave-Assisted Synthesis, Optical and Theoretical Characterization of Novel 2-(imidazo[1,5-a]pyridine-1-yl)pyridinium Salts. Chemistry 2021;3:714–27. https://doi.org/10.3390/chemistry3030050.
[33] Weber MD, Garino C, Volpi G, Casamassa E, Milanesio M, Barolo C, et al. Origin of a counterintuitive yellow light-emitting electrochemical cell based on a blue-emitting heteroleptic copper(I) complex. Dalton Trans 2016;45:8984–93. https://doi.org/10.1039/C6DT00970K.
[34] Volpi G, Garino C, Fresta E, Casamassa E, Giordano M, Barolo C, et al. Strategies to increase the quantum yield: Luminescent methoxylated imidazo[1,5-a]pyridines. Dyes Pigments 2021;192:109455. https://doi.org/10.1016/j.dyepig.2021.109455.
[35] Yamaguchi E, Shibahara F, Murai T. 1-Alkynyl- and 1-Alkenyl-3-arylimidazo[1,5-a]pyridines: Synthesis, Photophysical Properties, and Observation of a Linear Correlation between the Fluorescent Wavelength and Hammett Substituent Constants. J Org Chem 2011;76:6146–58.
[36] Ardizzoia GA, Brenna S, Durini S, Therrien B, Veronelli M. Synthesis, Structure, and Photophysical Properties of Blue-Emitting Zinc(II) Complexes with 3-Aryl-Substituted 1-Pyridylimidazo[1,5- *a*]pyridine Ligands: Blue-Emitting Zinc(II) Complexes. Eur J Inorg Chem 2014;2014:4310–9. https://doi.org/10.1002/ejic.201402415.
[37] Ardizzoia GA, Colombo G, Therrien B, Brenna S. Tuning the Fluorescence Emission and HOMO-LUMO Band Gap in Homoleptic Zinc(II) Complexes with N,O-Bidentate (Imidazo[1,5-a]pyrid-3-yl)phenols. Eur J Inorg Chem 2019;2019:1825–31. https://doi.org/10.1002/ejic.201900067.
[38] Volpi G, Lace B, Garino C, Priola E, Artuso E, Cerreia Vioglio P, et al. New substituted imidazo[1,5-a]pyridine and imidazo[5,1-a]isoquinoline derivatives and their application in fluorescence cell imaging. Dyes Pigments 2018;157:298–304. https://doi.org/10.1016/j.dyepig.2018.04.037.
[39] Thakare PP, Dakhane S, Shikh AN, Modak M, Patil A, Bobade VD, et al. Design, Synthesis, Antimicrobial and Ergosterol Inhibition Activity of New 4-(Imidazo[1,2-a]Pyridin-2-yl)Quinoline Derivatives. Polycycl Aromat Compd 2022;42:5282–99. https://doi.org/10.1080/10406638.2021.1933107.
[40] Perin N, Martin-Kleiner I, Nhili R, Laine W, David-Cordonnier M-H, Vugrek O, et al. Biological activity and DNA binding studies of 2-substituted benzimidazo[1,2-a]quinolines bearing different amino side chains. MedChemComm 2013;4:1537. https://doi.org/10.1039/c3md00193h.
[41] Hranjec M, Kralj M, Piantanida I, Sedić M, Šuman L, Pavelić K, et al. Novel Cyano- and Amidino-Substituted Derivatives of Styryl-2-Benzimidazoles and Benzimidazo[1,2- *a*]quinolines. Synthesis, Photochemical Synthesis, DNA Binding, and Antitumor Evaluation, Part 3. J Med Chem 2007;50:5696–711. https://doi.org/10.1021/jm070876h.
[42] Herr JM, Rössiger C, Albrecht G, Yanagi H, Göttlich R. Solvent-free microwave-assisted synthesis of imidazo[1,5- *a*]pyridine and –quinoline derivatives. Synth Commun 2019:1–10. https://doi.org/10.1080/00397911.2019.1650188.
[43] Cerrato V, Volpi G, Priola E, Giordana A, Garino C, Rabezzana R, et al. Mono-, Bis-, and Tris-Chelate Zn(II) Complexes with Imidazo[1,5-a]pyridine: Luminescence and Structural Dependence. Molecules 2023;28:3703. https://doi.org/10.3390/molecules28093703.
[44] Wang J, Mason R, VanDerveer D, Feng K, Bu XR. Convenient Preparation of a Novel Class of Imidazo[1,5-a]pyridines: Decisive Role by Ammonium Acetate in Chemoselectivity. J Org Chem 2003;68:5415–8. https://doi.org/10.1021/jo0342020.
[45] Sterckx H, De Houwer J, Mensch C, Herrebout W, Tehrani KA, Maes BUW. Base metal-catalyzed benzylic oxidation of (aryl)(heteroaryl)methanes with molecular oxygen. Beilstein J Org Chem 2016;12:144–53. https://doi.org/10.3762/bjoc.12.16.
[46] Jafarpour F, Ashtiani PT. A Novel One-Step Synthesis of Imidazo[5,1- *a*]isoquinolines via a Tandem Pd-Catalyzed Alkylation−Direct Arylation Sequence. J Org Chem 2009;74:1364–6. https://doi.org/10.1021/jo802584f.
[47] Albrecht G, Rössiger C, Herr JM, Locke H, Yanagi H, Göttlich R, et al. Optimization of the Substitution Pattern of 1,3-Disubstituted Imidazo[1,5- *a*]Pyridines and -Quinolines for Electro-Optical Applications. Phys Status Solidi B 2020;257:1900677. https://doi.org/10.1002/pssb.201900677.

[48] Colombo G, Cinco A, Ardizzoia GA, Brenna S. Long-Alkyl Chain Functionalized Imidazo[1,5-a]pyridine Derivatives as Blue Emissive Dyes. Colorants 2023;2:179–93. https://doi.org/10.3390/colorants2020012.
[49] Colombo G, Attilio Ardizzoia G, Brenna S. Imidazo[1,5-a]pyridine-based derivatives as highly fluorescent dyes. Inorganica Chim Acta 2022;535:120849. https://doi.org/10.1016/j.ica.2022.120849.
[50] Shibahara F, Kitagawa A, Yamaguchi E, Murai T. Synthesis of 2-Azaindolizines by Using an Iodine-Mediated Oxidative Desulfurization Promoted Cyclization of N-2-Pyridylmethyl Thioamides and an Investigation of Their Photophysical Properties. Org Lett 2006;8:5621–4. https://doi.org/10.1021/ol0623623.
[51] Yagishita F, Kozai N, Nii C, Tezuka Y, Uemura N, Yoshida Y, et al. Synthesis of Dimeric Imidazo[1, 5- *a*]pyridines and Their Photophysical Properties. ChemistrySelect 2017;2:10694–8. https://doi.org/10.1002/slct.201702277.
[52] Volpi G, Magistris C, Garino C. FLUO-SPICES: natural aldehydes extraction and one-pot reaction to prepare and characterize new interesting fluorophores. Educ Chem Eng 2018;24:1–6. https://doi.org/10.1016/j.ece.2018.06.002.
[53] Shibahara F, Sugiura R, Yamaguchi E, Kitagawa A, Murai T. Synthesis of Fluorescent 1,3-Diarylated Imidazo[1,5-a]pyridines: Oxidative Condensation-Cyclization of Aryl-2-Pyridylmethylamines and Aldehydes with Elemental Sulfur as an Oxidant. J Org Chem 2009;74:3566–8.
[54] Tverdiy D, Chekanov M, Savitskiy P, Syniugin A, Yarmoliuk S, Fokin A. Efficient Preparation of Imidazo[1,5-a]pyridine-1-carboxylic Acids. Synthesis 2016;48:4269–77. https://doi.org/10.1055/s-0035-1561489.
[55] Chandrasekar S, Sangeetha S, Sekar G. Synthesis of 1,3-Disubstituted Imidazo[1,5- *a*]pyridines through Oxidative C-N Bond Formation from Aryl-2-pyridylmethanols and Their Fluorescent Study. ChemistrySelect 2019;4:5651–5. https://doi.org/10.1002/slct.201901440.
[56] Renno G, Cardano F, Volpi G, Barolo C, Viscardi G, Fin A. Imidazo[1,5-a]pyridine-Based Fluorescent Probes: A Photophysical Investigation in Liposome Models. Molecules 2022;27:3856. https://doi.org/10.3390/molecules27123856.
[57] Shibahara F, Yamaguchi E, Kitagawa A, Imai A, Murai T. Synthesis of 1,3-diarylated imidazo[1,5-a]pyridines with a combinatorial approach: metal-catalyzed cross-coupling reactions of 1-halo-3-arylimidazo[1,5-a]pyridines with arylmetal reagents. Tetrahedron 2009;65:5062–73. https://doi.org/10.1016/j.tet.2009.02.062.
[58] Yamaguchi E, Shibahara F, Murai T. 1-Alkynyl- and 1-Alkenyl-3-arylimidazo[1,5- *a*]pyridines: Synthesis, Photophysical Properties, and Observation of a Linear Correlation between the Fluorescent Wavelength and Hammett Substituent Constants. J Org Chem 2011;76:6146–58. https://doi.org/10.1021/jo200864x.
[59] Taniya OS, Fedotov VV, Novikov AS, Sadieva LK, Krinochkin AP, Kovalev IS, et al. Abnormal push-pull benzo[4,5]imidazo[1,2-a][1,2,3]triazolo[4,5-e]pyrimidine fluorophores in planarized intramolecular charge transfer (PLICT) state: Synthesis, photophysical studies and theoretical calculations. Dyes Pigments 2022;204:110405. https://doi.org/10.1016/j.dyepig.2022.110405.
[60] Jiang G, Li Q, Lv A, Liu L, Gong J, Ma H, et al. Modulation of the intramolecular hydrogen bonding and push–pull electron effects toward realizing highly efficient organic room temperature phosphorescence. J Mater Chem C 2022;10:13797–804. https://doi.org/10.1039/D2TC01093C.
[61] Doval DA, Molin MD, Ward S, Fin A, Sakai N, Matile S. Planarizable push–pull oligothiophenes: in search of the perfect twist. Chem Sci 2014;5:2819–25. https://doi.org/10.1039/C4SC00939H.
[62] Grimm JB, Lavis LD. Caveat fluorophore: an insiders' guide to small-molecule fluorescent labels. Nat Methods 2022;19:149–58. https://doi.org/10.1038/s41592-021-01338-6.
[63] Fu Y, Finney NS. Small-molecule fluorescent probes and their design. RSC Adv 2018;8:29051–61. https://doi.org/10.1039/C8RA02297F.
[64] Giordano M, Volpi G, Bonomo M, Mariani P, Garino C, Viscardi G. Methoxy-substituted copper complexes as possible redox mediators in dye-sensitized solar cells. New J Chem 2021;45:15303–11. https://doi.org/10.1039/D1NJ02577E.
[65] Volpi G, Garino C, Salassa L, Fiedler J, Hardcastle KI, Gobetto R, et al. Cationic Heteroleptic Cyclometalated Iridium Complexes with 1-Pyridylimidazo[1,5-alpha]pyridine Ligands: Exploitation of

an Efficient Intersystem Crossing. Chem- Eur J 2009;15:6415–27. https://doi.org/10.1002/chem.200801474.
[66] Salassa L, Garino C, Albertino A, Volpi G, Nervi C, Gobetto R, et al. Computational and spectroscopic studies of new rhenium(I) complexes containing pyridylimidazo[1,5-a]pyridine ligands: Charge transfer and dual emission by fine-tuning of excited states. Organometallics 2008;27:1427–35. https://doi.org/10.1021/om701175z.
[67] Volpi G, Magistris C, Garino C. Natural aldehyde extraction and direct preparation of new blue light-emitting imidazo[1,5-a]pyridine fluorophores. Nat Prod Res 2018;32:2304–11. https://doi.org/10.1080/14786419.2017.1410803.
[68] Volpi G, Garino C, Conterosito E, Barolo C, Gobetto R, Viscardi G. Facile synthesis of novel blue light and large Stoke shift emitting tetradentate polyazines based on imidazo[1,5-a]pyridine. Dyes Pigments 2016;128:96–100. https://doi.org/10.1016/j.dyepig.2015.12.005.
[69] Volpi G, Garino C, Priola E, Diana E, Gobetto R, Buscaino R, et al. Facile synthesis of novel blue light and large Stoke shift emitting tetradentate polyazines based on imidazo[1,5-a]pyridine – Part 2. Dyes Pigments 2017;143:284–90. https://doi.org/10.1016/j.dyepig.2017.04.034.
[70] Volpi G, Galliano S, Buscaino R, Viscardi G, Barolo C. Fluorescent trifluoromethylated imidazo[1,5-a]pyridines and their application in luminescent down-shifting conversion. J Lumin 2022;242:118529. https://doi.org/10.1016/j.jlumin.2021.118529.
[71] Frisch MJ, Trucks GW, Schlegel HB, Scuseria GE, Robb MA, Cheeseman JR, et al. Gaussian 16 2016.
[72] Stratmann RE, Scuseria GE, Frisch MJ. An efficient implementation of time-dependent density-functional theory for the calculation of excitation energies of large molecules. J Chem Phys 1998;109:8218–24. https://doi.org/10.1063/1.477483.
[73] Casida ME, Jamorski C, Casida KC, Salahub DR. Molecular excitation energies to high-lying bound states from time-dependent density-functional response theory: Characterization and correction of the time-dependent local density approximation ionization threshold. J Chem Phys 1998;108:4439–49. https://doi.org/10.1063/1.475855.
[74] Becke AD. Density-functional thermochemistry. III. The role of exact exchange. J Chem Phys 1993;98:5648–52. https://doi.org/10.1063/1.464913.
[75] Lee CT, Yang WT, Parr RG. Development of the Colle-Salvetti Correlation-Energy Formula into a Functional of the Electron-Density. Phys Rev B 1988;37:785–9. https://doi.org/10.1103/PhysRevB.37.785.
[76] McLean AD, Chandler GS. Contracted Gaussian basis sets for molecular calculations. I. Second row atoms, Z=11–18. J Chem Phys 1980;72:5639–48. https://doi.org/10.1063/1.438980.
[77] Cossi M, Scalmani G, Rega N, Barone V. New developments in the polarizable continuum model for quantum mechanical and classical calculations on molecules in solution. J Chem Phys 2002;117:43–54. https://doi.org/10.1063/1.1480445.
[78] Miertus S, Scrocco E, Tomasi J. Electrostatic interaction of a solute with a continuum. A direct utilizaion of AB initio molecular potentials for the prevision of solvent effects. Chem Phys 1981;55:117–29.
[79] O'boyle NM, Tenderholt AL, Langner KM. cclib: A library for package-independent computational chemistry algorithms. J Comput Chem 2008;29:839–45. https://doi.org/10.1002/jcc.20823.
[80] Browne WR, O'Boyle NM, McGarvey JJ, Vos JG. Elucidating excited state electronic structure and intercomponent interactions in multicomponent and supramolecular systems. Chem Soc Rev 2005;34:641–63. https://doi.org/10.1039/B400513A.
[81] Headgordon M, Grana AM, Maurice D, White CA. Analysis of Electronic-Transitions as the Difference of Electron-Attachment and Detachment Densities. J Phys Chem 1995;99:14261–70. https://doi.org/10.1021/j100039a012.
[82] Pettersen EF, Goddard TD, Huang CC, Couch GS, Greenblatt DM, Meng EC, et al. UCSF Chimera--a visualization system for exploratory research and analysis. J Comput Chem 2004;25:1605–12. https://doi.org/10.1002/jcc.20084.